Rewired NAD^+ metabolism promotes NF-κB-mediated oxidative stress and disrupts lipid homeostasis in liver fibrosis progression

Hiu-Lok Ngan,[1] Jacinth Wing-Sum Cheu,[2,3] Kenneth Kin-Leung Kwan,[2,3] Carmen Chak-Lui Wong,[2,3,*] Hong Yan,[1,4,*] Zongwei Cai[1,5,*]

[1]State Key Laboratory of Environmental and Biological Analysis, Department of Chemistry, Hong Kong Baptist University, Hong Kong, P. R. China

[2]State Key Laboratory of Liver Research, Department of Pathology, Li Ka Shing Faculty of Medicine, The University of Hong Kong, Hong Kong, P. R. China

[3]Centre for Oncology and Immunology, Hong Kong Science Park, Hong Kong, P. R. China

[4]Department of Biology, Hong Kong Baptist University, Hong Kong, P. R. China

[5]College of Science, Eastern Institute of Technology, Ningbo, China

***Corresponding authors: Drs. Carmen Chak-Lui Wong, Hong Yan, and Zongwei Cai**

Emails: carmencl@pathology.hku.hk; hongyan@hkbu.edu.hk; zwcai@hkbu.edu.hk

ABSTRACT

Chronic liver fibrosis is a major risk factor for the development of hepatocellular carcinoma (HCC), a leading cause of cancer deaths worldwide. However, the underlying molecular mechanisms linking fibrosis to inflammation-associated HCC development remain elusive, hindering early diagnosis and intervention. In this study, we combined unbiased multi-omics analyses, including metabolomics, lipidomics, and transcriptomics, in a mouse model of chemical-induced liver fibrosis and HCC, and integrated publicly available transcriptome data from LX-2 human hepatic stellate cell (HSC) line. Our results revealed a profound rewiring of NAD^+ metabolism as a central driver of metabolic disturbance. Multi-omics analysis of the bulk liver tissue showed increased activity of the kynurenine pathway of tryptophan metabolism, boosting the production of NAD^+ precursors. Hepatic nicotinamide (NAM) level decreased due to the elevated expression of NAM *N*-methyltransferase (*Nnmt*) in HSCs. Despite the decreased hepatic NAM, serum NAD^+ level was compartmentalized, with increased NAD^+ in circulation, and hepatic sirtuins, including *Sirt1*, were downregulated to reduce conversion of NAD^+ into NAM. This NAM consumption/salvage imbalance derived the disruption of NAD^+ homeostasis, triggering the activation of NF-κB-mediated oxidative stress pathways. Furthermore, lipid dysregulation was evidenced by the domination of NF-κB regulation to SIRT1/SREBP-controlled lipogenic and cholesterogenic genes, leading to hepatic and serum lipid imbalance. These multi-omics insights elucidate mechanistic links between rewired NAD^+ metabolism, inflammation, and lipid dysregulation during fibrosis-HCC progression. Our findings may facilitate the development of novel diagnostic biomarkers and therapeutic targets for this deadly disease.

KEYWORDS

hepatocellular carcinoma | cirrhosis | hepatic stellate cells | nicotinamide | sirtuin 1 | *de novo* lipogenesis | multi-omics

SIGNIFICANCE

The transition from chronic liver scarring to liver cancer is a major health concern, yet the underlying mechanisms have been poorly understood. This study used multi-omics approach to uncover a key driver of this dangerous progression – disruptions in the metabolism of an important molecule called NAD^+. We found that changes in the pathways that produce and recycle NAD^+ led to an imbalance, with increased NAD^+ precursors but decreased levels of the NAD^+ byproduct nicotinamide. This NAD^+ homeostasis breakdown triggered harmful inflammation and alterations in lipid metabolism. These new insights into the molecular underpinnings could enable early cancer diagnosis by deploying disease progression biomarkers and intervention by correcting the disrupted NAD^+ metabolism.

INTRODUCTION

Cancer represents a significant global health burden, according for nearly 10 million deaths worldwide in 2020 (1). Among the various cancer types, liver cancer stands out as a particularly devastating chronic disease and is the emerging one in the United States (2). While ranking 7th in incidence, it was the 3rd leading cause of cancer-related mortality (3), with a strikingly high mortality-to-incidence ratio of nearly 1:1 (3). This underscores the lethality of liver cancer compared to other malignancies.

Early detection and intervention are critical for improving patient outcomes, yet liver cancer is often diagnosed at advanced stages, less treatable stages (4). Hepatocellular carcinoma (HCC) is the most common subtype of liver cancer (5). Its risk factors mostly are related to cirrhosis (6), that can be induced by hepatitis B virus (HBV) and hepatitis C virus, alcohol, and metabolism-associated factors, such as diabetes, obesity, non-alcoholic fatty liver disease (NAFLD) (7). Chronic liver injury triggers a sustained wound-healing response characterized by the activation and differentiation of hepatic stellate cells (HSCs) into collagen-producing myofibroblasts, leading to the progressive scarring of the liver known as fibrosis (8). Advanced liver fibrosis results in cirrhosis and involves in hepatocarcinogenesis (9). Hence, elucidating the fibrosis-dependent mechanisms driving tumor progression will be crucial to rationalizing the development of antifibrotic therapies as an early intervention strategy.

The current body of clinical research of inflammation-associated HCC has primarily focused on analyzing serum samples from patients diagnosed with HCC (10–13), cirrhosis (13, 14), fibrosis (15), or HBV infection (10, 13). Serum metabolomics is advantageous for the discovery of diagnostic biomarkers due to its relatively non-invasive sampling approach. However, in the context of early detection and disease intervention, tissue samples are necessary to examine the underlying molecular underpinnings driving the transition from chronic liver disease. Unfortunately, the availability of clinical tissue samples is often limited

to the advanced stage of disease at the time of diagnosis. While there are several studies on HCC (10, 13, 16, 17) and cirrhosis (18), tissue samples from the fibrotic stage are scarce (19). This limitation in access to well-characterized fibrotic tissue samples represents a significant challenge that hinders our understanding of the fibrosis-dependent tumorigenic mechanisms. To fill this knowledge gap, animal models of liver fibrosis and inflammation-associated HCC are needed for a comprehensive investigation of the metabolic, signaling, and regulatory alterations in rodent liver tissue prior to clinical investigation (20, 21).

In this study, we employ a diethylnitrosamine-carbon tetrachloride (DEN-CCl_4) chemical-induced male mouse model to monitor the etiology and progression of fibrosis-associated HCC by multi-omics analyses, including inter-validation between metabolomics, lipidomics, and transcriptomics and external validation by a transcriptome set of activated human HSCs. We characterize metabolic disturbances in tryptophan metabolism, nicotinate/nicotinamide metabolism, fatty acid (FA) metabolism, alanine/aspartate/glutamate (AAG) metabolism, and citrate cycle throughout the progression stages (fibrosis, cirrhosis, and HCC) and identify several potential diagnostic serum and tissue biomarkers for disease monitoring. We confirm the dysregulated metabolic pathways discovered through our multi-omics analyses using RNA sequencing (RNA-Seq) and assess their occurrence and regulation within HSCs. Overall, our results demonstrate NAM depletion by the upregulation of NAM *N*-methyltransferase (*Nnmt*) in HSCs derives the rewiring of nicotinamide adenine dinucleotide (NAD^+) metabolism. Disturbances in NAD^+ homeostasis and its associated pathways trigger inflammation and lipid dysregulation, that create a pro-tumorigenic microenvironment in the fibrotic liver. These findings may ultimately contribute to improved early detection and more effective interventions to prevent the devastating progression from chronic liver disease to HCC.

RESULTS

Untargeted Metabolomics and Global Transcriptomics Identify Hepatic Fibrosis-Cirrhosis-HCC Progression-Related Metabolic Pathways.

We initiated our study by untargeted multi-omics analyses, including reverse-phase liquid chromatography/mass spectrometry (RPLC/MS)-based metabolomics and RNA-Seq, to discover the main metabolic disturbances that occur during the progression from liver fibrosis to cirrhosis and eventual HCC using the DEN-CCl_4 mouse model. At each disease stage, omics data of the diseased mice were evaluated against the data of age-matched controls (AMCs). For metabolite identification at this point, the confidence level followed the criteria of level 2B of the Metabolomics Standards Initiative (22), implying that the mass-to-charge ratio (*m/z*) values of the annotated metabolites' molecular ions were matched with the chemical standards' values registered in mass spectral libraries. A collection of annotated metabolites exhibited disease stage-specific significant differences and fold changes compared to their corresponding AMCs (Fig. 1 *A–B*), including lipids. Notably, their altered levels were not due to any systematic error during LC/MS assay, as all injections for quality control (QC) in both positive (Fig. 1*A*) and negative (Fig. 1*B*) electrospray ionization (ESI) mode were assessed to have tolerable relative standard derivations (RSDs) of < 30% (23).

Metabolite set enrichment analyses on the untargeted metabolomics data showed a list of pathways were significant and agreed with the pathway enrichment results of RNA-Seq (Fig. 2 *A–B*). Several significant pathways (i.e., AAG metabolism, tryptophan metabolism, and citrate cycle) in fibrosis (Fig. 2 *A–B*) were also discriminative in cirrhosis (Fig. 2*C*) and HCC (Fig. 2*D*). Together with nicotinate/nicotinamide metabolism (Fig. 2 *C–D*), they were all NAD^+- or energy metabolism -related pathways. Targeted metabolomics was then performed to relatively quantify these compound metabolites in bulk liver tissue samples and serum,

accompanied by lipidomics since FA metabolism was also enriched in global transcriptomics and relevant to energy metabolism (Fig. 2*B*).

Integration of Targeted Metabolomics and RNA Sequencing Reveals Decreased Hepatic Nicotinamide Levels Despite Upregulation of *De Novo* NAD^+ Synthesis.

To further explore the disturbances in NAD^+ metabolism identified in the untargeted analyses, we performed targeted RPLC/tandem MS on rodent liver tissue samples. This revealed the metabolites of the kynurenine pathway of tryptophan metabolism were significantly increased in fibrotic livers (Fig. 3 *A–B* and Dataset S1). Transcriptomic analysis showed that all the genes encoding regulatory enzymes were significant upregulated as differentially expressed gene (DEGs) during fibrogenesis (Fig. 3*A* and Table 1), especially the overexpression of the rate-limiting enzyme tryptophan 2,3-dioxygenase (*Tdo2*). This finding aligns with the results of tryptophan-kynurenine pathway upregulation reported by Hoshi *et al.* in their CCl_4-induced fibrotic mouse livers (24).

Our targeted analysis also indicated a continuous, significant decrease in hepatic nicotinamide (NAM) levels across the fibrosis-cirrhosis-HCC disease progression (Fig. 3 *A* and *C* and Dataset S1), despite a significant upregulation of the *de novo* NAD^+ synthesis pathway (Fig. 3 *A–C* and Dataset S1). The RNA-Seq data for fibrosis agreed with the depletion of the available hepatic NAM pool, which was attributed to the increased expression of the NAM *N*-methyltransferase (*Nnmt*) gene (Table 1), catalyzing the methylation of NAM and resulting in a significant increase of the downstream end-product *N*-methyl-4-pyridone-3-carboxamide (Fig. 3 *A* and *C* and Dataset S1). Furthermore, we overserved downregulation of genes encoding the Sirtuin (SIRT) family of NAD^+-dependent deacetylases, as well as the rate-limiting enzyme NAM phosphoribosyltransferase (*Nampt*) in the NAD^+ salvage pathway (Table 1). In contrast, the expression of NAM mononucleotide adenylyltransferase 1 (*Nmnat1*), which catalyzes the final step of *de novo* NAD^+ synthesis, was upregulated. The association

between the imbalance of NAM consumption/salvage and liver fibrosis via SIRT and NAD^+ metabolism, as reported by Komatsu *et al.* (25), consolidates our findings on the nicotinate and NAM metabolism.

Rewiring of NAD^+ Metabolism Dysregulates NAD^+-Dependent Pathways.

The observed disturbances in NAD^+ homeostasis, driven by the depletion of the salvage pathway substrate NAM, prompted us to further investigate the downstream impact on NAD^+-dependent pathways, including FA metabolism, citrate cycle, and AAG metabolism, during the fibrosis-associated HCC progression (26). Our targeted metabolomics and lipidomics analyses revealed significant upregulation of FA beta-oxidation, as evidence by the progressive decrease of the free medium-chain saturated FA (9:0) and long-chain saturated free FAs, palmitate and stearate, and the increase in the acylcarnitine pool level (Fig. 3 *A* and *D* and Datasets S1 and S2). The transcriptomics data indicated an increased expression of a cascade of DEGs encoding enzymes involved in FA oxidation (FAO) (Fig. 3*A* and Table 1), including the rate-limiting enzymes carnitine palmitoyltransferase 1A (*Cpt1a*), suggesting a shift towards the utilization of straight-chain free FAs as an energy source (27). Moreover, we observed significantly increased levels of asparagine, aspartate, glutamine, and glutamate in the AAG metabolism pathway (Fig. 3 *A* and *E* and Dataset S1) and a slightly upregulation of most citrate cycle intermediates (Fig. 3 *A* and *F* and Dataset S1). The RNA-Seq data showed that all the related DEGs were significantly overexpressed in these metabolic pathways, corroborating the alterations observed in the targeted metabolomics data (Table 1). Our findings of increased hepatic acylcarnitine and elevated TCA cycle activity were collectively aligned with the results reported by Satapati *et al.*, which demonstrated that mitochondrial citrate cycle anaplerosis was dysregulated by the upregulation of gluconeogenesis in high-fat diet male mice with obesity and hepatic insulin resistance (28).

Several Potential Diagnostic Tissue and Serum Metabolite Biomarkers Are Suggested for Disease Monitoring or Detection.

The integration of the targeted metabolomics and transcriptomics data, along with the comparative analysis of liver tissue and serum samples, allowed us to identify several potential diagnostic biomarkers that could be feasible for monitoring the progression of liver disease. Our analyses revealed a panel of potential tissue biomarkers that could be suitable for fine-needle biopsy assessment (Fig. 3 *A–F* and Datasets S1 and S2), including the upregulation of serotonin and indoleacetate (Fig. 3*B*), the depletion of NAM, and the increase of quinolinate, *N*-methyl-4-pyridone-3-carboxamide (Fig. 3*C*), the consumption of straight-chain FAs, the accumulation of acylcarnitine level, ceramide level (Fig. 3*D*), glutamate (Fig 3*E*), as well as the citrate cycle intermediates like 2-oxo-glutarate, malate, and fumarate (Fig. 3*F*). The elevated levels of indoleacetate (*SI Appendix*, Fig. S1*A*), quinolinate (*SI Appendix*, Fig. S1*B*), acylcarnitine (*SI Appendix*, Fig. S1*C*), glutamate (*SI Appendix*, Fig. S1*D*), and 2-oxo-glutarate (*SI Appendix*, Fig. S1*E*), and the decreased level of NAM (*SI Appendix*, Fig. S1*B*) and straight-chain FAs (*SI Appendix*, Fig. S1*C*) were aligned with the results of liver biopsies collected from patients diagnosed with HCC (Dataset S3). These tissue biomarkers thus have the potential for translational application.

As primary bile acid (BA) biosynthesis was also one of the significant pathways in fibrosis-associate HCC progression (Fig 2 *A* and *C–D*), primary BAs were analyzed in rodent and clinical liver samples. Taurochenodeoxycholate and taurocholate showed progressive increases at each disease stage in the DEN-CCl_4 mice (Dataset S1 and *SI Appendix*, Fig. S2*A*), while they were not detected in the human liver samples (Dataset S3 and *SI Appendix*, Fig. S2*B*). Among the detectable BAs, chenodeoxycholate showed significant difference from the controls in the HCC stage in rodent and clinical samples, but not progressive alterations in the rodent samples

(Datasets S1 and S3 and *SI Appendix*, Fig. S2 *A–B*). The total BA content showed no significant changes at each stage (*SI Appendix*, Fig. S3).

Serum BAs had no predictable pattern along the fibrosis-associated HCC progression. Chenodeoxycholate, cholate, glycochenodeoxycholate, and glycocholate showed only stage-specific significances (Datasets S4 and *SI Appendix*, Fig. S2*C*). Despite the lack of discovery of novel serum BA biomarkers, our result of glycocholate increment was in agreement with the previously reported data from another group (29).

Besides serum BAs, we identified potential serum metabolite biomarkers with progressive changes that could provide a relatively non-invasive approach for early diagnosis (Fig. 4 *A–C* and Dataset S4), such as the decreased levels of 5-hydroxytryptophan and serotonin (Fig. 4*B*), and the elevated level of quinolinate (Fig. 4*C*). High level of serum quinolinate has been found in liver cirrhosis patients with systematic inflammation (30). Tryptophan, which was proposed as a potential serum biomarker by previous reports on the perturbations of tryptophan metabolism during hepatic fibrosis progression in rodent models (29), was altered with progressive increase along fibrosis-cirrhosis-HCC staging, if its relative intensity to the AMC at each disease stage is neglected.

Disturbances in NAD^+ Homeostasis and Its Associated Pathways Trigger Pro-Inflammatory Consequences.

The disturbances in NAD^+ homeostasis and the associated dysregulation of NAD^+-dependent pathways during liver disease progression prompted us to further investigate the potential pro-inflammatory consequences using data from the transforming growth factor beta 1 (TGF-β1)-activated human HSC cell line LX-2 cell (31). This is because the activation of HSCs, which involves the transformation of quiescent cells into proliferative, matrix-producing myofibroblasts, is recognised as a pivotal mechanism driving fibrosis in both experimental and clinical liver disease models (32). Our transcriptomic analysis of the bulk rodent liver samples

and TGF-β1-stimulated LX-2 cells revealed that the upregulation of tryptophan metabolism and serotonin synthesis may not be located within the HSCs, or the expression patterns may be temporally dissociated (Fig. 5*A*). The NAD^+ metabolism dysregulation appears to occur at an earlier stage, while the tryptophan pathway upregulation could be a later adaptive response during liver fibrogenesis. In the activated LX-2 cells, the overexpression of the DEGs, including 3-hydroxyanthranilate (3-HAA) 3,4-dioxygenase (*Haao*), quinolinate phosphoribosyl transferase (*Qprt*), *Cd38*, and nuclear factor kappa B subunit 1 (*Nfkb1*), was consistent with the RNA-Seq data from our *in vivo* studies (Fig. 5 *A*, *B*, *D*, and *F* and Table 1). Also, the downregulated genes in the *in vitro* studies, such as the AMPK regulatory subunit 5'-AMP-activated protein kinase subunit gamma-2 (*Prkag2*), *Nnmt*, *Sirt1*, and aldehyde oxidase 1 (*Aox1*), were also identified as the DEGs in the rodent fibrotic liver samples (Fig. 5 *A–C* and *E* and Table 1).

In the HSCs, the overexpression of *Nnmt*, which catalyzes the methylation of NAM, led to the accumulation of *N*1-methyl NAM. This NAM depletion was further exacerbated by the downregulation of *Aox1* (Fig. 5 *A–C* and *E* and Table 1). The decreased NAM availability was intensified by the downregulation of *Sirt1* and AMPK/PRKAG2, leading to impaired NAM salvage. The reduced *Sirt1* activity also diminished the silencing of pro-inflammatory NF-κB signaling. Together with the upregulation of CD38, the inactivation of AMPK promoted the activation of pro-inflammatory pathways. Notably, PRKAG2 variants have been associated with liver cirrhosis (33), and 3-HAA has been reported to regulate inflammasome activation (34), further supporting our collective findings.

Downregulated AMPK Signaling Pathway Triggers Lipid Homeostasis Imbalance.

Our metabolite set enrichment analyses revealed that the sphingolipid metabolism pathway was significantly perturbed in the early stages of fibrosis and cirrhosis (Fig. 2 *A* and *C*). The differential expression of key genes involved in the ceramide biosynthetic pathway was notably

upregulated (Fig. 3 *A* and *D* and Table 1). Meanwhile, the significant differences in acylcarnitine, a marker of FAO, relative to the levels in the AMCs was also observed (Fig. 3 *A* and *D*), suggesting a strong propensity for FA catabolism. This is supported by the evidence that the presence of *Cpt1a*, the rate-limiting enzyme in beta-oxidation, is crucial for the activation of HSCs (27). Elevated expression of *Cpt1a* was reported in the HSCs of patients with non-alcoholic steatohepatitis (NASH), along with a positive correlation with the hepatic fibrosis score (27). Upon activation, HSCs begin to lose their intracellular FA stores. Interestingly, the expression of *Cpt1a* was downregulated in the TGF-β1-stimulated LX-2 cells after 24 hours of incubation (Table 1), contrasting with its upregulation during the earlier stages of activation (from 1 to 12 hours of incubation) reported by Fondevila *et al.* (27). Our transcriptomic analysis of the bulk rodent liver samples and *in vitro* studies revealed that the upregulation of FAO may be temporally dissociated (Fig. 6*A*), occurring at an earlier stage, while the steroid biosynthesis upregulation could be a later adaptive response during liver fibrogenesis.

In the activated HSCs, the overexpression of the DEGs, including ATP citrate lyase (*Acly*) and FA synthase (*Fasn*) in *de novo* lipogenesis (DNL), acyl-CoA:cholesterol acyltransferase 2 (*Acat2*), 3-hydroxy-3-methylglutaryl-CoA synthase 1 (*Hmgcs1*), sterol regulatory element-binding protein 2 (*Srebf2*), and a cascade of genes in the mevalonate pathway of cholesterogenesis, including 3-Hydroxy-3-methylglutaryl-CoA reductase (*Hmgcr*), was consistent with the RNA-Seq data from our *in vivo* studies (Fig. 6 *A*, *B*, *D*, and *F* and Table 1). Both *in vivo* and *in vitro* studies showed the downregulations of the AMPK-SIRT1 axis and the consequent derepression of the sterol regulatory element-binding proteins (SREBPs), which are key transcriptional regulators of DNL and cholesterogenesis in HSCs (Fig. 6 *A–C`* and *E* and Table 1) (35). This resulted in the overexpression of genes *Acly* and *Fasn*, as well as those

involved in cholesterol biosynthesis, in line with the fact that lipogenesis required the overexpression of the rate-limiting enzyme *Fasn* in mouse models of obesity and NAFLD (36).

DISCUSSION

In this comprehensive multi-omics study, we have revealed the major metabolic pathways and signaling networks that are dysregulated during liver fibrosis and inflammation-associated HCC progression. The integration of untargeted metabolomics, targeted metabolomics, lipidomics, and global transcriptomics has provided a holistic understanding of the metabolic rewiring that occurs in the early stages of liver fibrogenesis. The key metabolic pathways identified to be dysregulated include NAD^+ metabolism, *de novo* NAD^+ biosynthesis, sphingolipid synthesis, FAO, DNL, and cholesterogenesis. Global transcriptomics in our *in vivo* studies validates the metabolic alterations by DEGs expression. The DEGs are double confirmed by the external RNA-Seq data of TGF-β1-treated LX-2 cells (31).

The importance of NAD^+ metabolism in regulating various cellular processes is well-established (26), and our study has revealed its significant dysregulation during liver disease progression. The state-specific changes in the levels of NAD^+ and its precursor, NAM, suggest a complex interplay between *de novo* NAD^+ synthesis, NAM salvage, and NAM clearance mechanisms. In the early stages of HCC progression (i.e., advanced fibrotic liver stages in fibrosis and cirrhosis), despite the upregulation of *de novo* NAD^+ synthesis, the hepatic NAM levels were decreased (Figs. 3 *A* and C and Dataset S1). This was due to the overexpression of *Nnmt* (Fig. 5 *A*, *B*, *D*, and *F* and Table 1), catalyzing the methylation of NAM. The overexpression of *Nnmt* was found during the progression of various cancers (37). Its correlation to the cancer-associated fibroblast was reported (38), yet our *in vitro* analysis demonstrated a comparative overexpression of the DEGs encoding NAD^+ metabolism in the activated HSCs, implying *Nnmt* has a central role of metabolic regulation of myofibroblast differentiation and cancer progression (38).

The accumulation of methylated NAM was exacerbated by the downregulation of *Aox1* (Fig. 5 *A–C* and *E* and Table 1), an enzyme responsible for the clearance of this methylated metabolite. As a "methyl sink" in carcinogenesis, NAM is methylated and eventually excreted from the body (39). Measurements of serum and urine methylated NAM was found to be significantly higher concentrations in patients with cirrhosis compared to healthy controls (40), suggesting that the impairment in NAM salvage mechanisms leads to the excessive clearance of this methylated metabolite from the body and decreased NAD^+ salvage.

Attempted recovery of NAM and NAD^+ was attained by the upregulation of the *de novo* NAD^+ synthesis. It was evidenced by a study on the depressed expression of NAM salvage in mice (41). Overexpression of *Haao* and *Qprt* were found in the HSCs (Fig. 5 *A*, *B*, *D*, and *F* and Table 1). This enzymatic upregulation led to the rapid production and consumption of quinolinate (Figs. 3 *A* and *C* and 4*A* and Dataset S1), suggesting a metabolic adaption to maintain hepatic NAD^+ levels. Upregulation of tryptophan-kynurenine pathway in liver was also reported in the consequence of hypoxia-causing manganese exposure (42). Despite the increased hepatic NAD^+ level observed (Fig. 1 *A* and *C* and Dataset S1), the system was unable to compensate for the loss of NAM, as the NAD^+ could not be efficiently converted back into NAM due to the downregulation of AMPK/PRKAG2 and SIRT1 (Fig. 5 *A–C* and *E* and Table 1). As a result, the excess NAD^+ was shunted into the systemic circulation. Increased serum NAD^+ levels in adults with metabolic diseases, including obesity and NAFLD was reported, and there was no significant interaction between age, sex, drinking, smoking, and NAD^+ for the metabolic diseases (43). The high blood NAD^+ level was not attributed from the non-hepatic NAD^+ (44), suggesting the circulating NAD^+ was contributed by the liver.

The decreased hepatic NAM levels, despite the upregulation of *de novo* NAD+ biosynthesis, contributed to the activation of pro-inflammatory signaling cascades in the HSCs through multiple mechanisms. Firstly, the downregulation of the AMPK-SIRT1 axis, resulting from the

NAM depletion and NAD^+ affluence, led to the derepression of NF-κB signaling (Fig. 5 *A*, *B*, *D*, and *F* and Table 1). While the decreased NAM levels and consequent impairment of this axis allowed for the unchecked activation of NF-κB in the HSCs. Additionally, the increased expression of CD38, being found on the surface of HSCs (45), further exacerbated the pro-inflammatory consequences. NAD^+ affluence has been reported by selectively inhibition of CD38 ectoenzyme, accompanying with significant prevention from fibrosis (46), partially through the mechanisms of blunting the recruitment of immune cells and NF-κB signaling (47). Several studies reported boosting hepatic NAD^+ level improved liver injury and inflammation by nicotinic acid (NA) riboside supplementation (44), or NA supplementation by converting NAM into NAD^+ (48), counteracting the activity of CD38 by that of NAMPT. However, targeting CD38 or upregulating NAMPT resulted to a similar effect as upregulation of tryptophan-kynurenine pathway, and might be not sufficient when AMPK-SIRT1 is still downregulated. Together, targeted interventions aimed at restoring NAM availability, modulating AMPK-SIRT1-NF-κB axis, and inhibiting CD38 activity may hold significant therapeutic potential for mitigating the inflammatory and fibrogenic processes.

Besides AMPK-SIRT1-NF-κB axis, our analysis revealed that rewiring of NAD^+ metabolism also resulted to imbalance in hepatic lipid homeostasis during the progression of liver disease through AMPK-SIRT1-NF-κB-SREBP axis in HSCs (49). The activity of SREBP2 was indicated that it can be regulated by 3-HAA metabolism (34). The key transcription factors involved in this lipid metabolism dysregulation are the SREBPs, which are substrates of SIRT1 enzyme (35). While the SREBP1a and SREBP1c isoforms (encoded by the *Srebf1* gene) are regulated by the AMPK-SIRT1 axis, the SREBP2 isoform (encoded by the *Srebf2* gene) is less susceptible to this repression (50). We observed the upregulation of key genes involved in the SREBP-regulated pathways of DNL and cholesterol biosynthesis (Fig. 6 *A*, *B*, *D*, and *F* and Table 1). This suggests a shift towards

increased synthesis of palmitate or other FAs, cholesterol, and sterol metabolites. Interestingly, despite this transcriptional upregulation, we detected decreased levels of palmitate and other FAs along the disease progression (Dataset 2). This indicated that the overall tendency in FA metabolism was towards the increased acylcarnitine formation and subsequent FAO (Fig. 3 *A* and *D* and Dataset S1). This could potentially be for the purpose of other lipid biosynthesis, such the observed upregulation of the sphingolipid signaling pathway (Fig. 3*A* and Table 1) and ceramide biosynthesis in the fibrosis and cirrhosis stages.

The overexpression of genes encoding FAO, including the rate-limiting enzyme *Cpt1a* was observed *in vivo* (Fig. 3*A* and Table 1). Expression of *Cpt1a* showed to be induced by the FAO-derived reactive oxygen species (27). In our *in vivo* studies, the FAO appears to be upregulated by the demands of saturated FAs, as reflected by the lipidomics data (Fig. 3 *A* and *D* and Dataset S2). Although our *in vitro* data analysis showed the activated HSCs might have a delayed response in FAO (Table 1), elevated expression of *Cpt1a* is a hallmark in HSC activation in the pathogenesis of hepatic fibrosis in patients with NASH, in rodents, and in TGF-β1-stimulated LX-2 cells incubated with saturated FAs-rich mediation (27). A study also showed that killer T cells-derived interferon gamma (IFN-γ) induces activation of FAO and *Cpt1a* upregulation in cancer cells in an AMPK-dependent manner (51). This can be used to explain why *Cpt1a* is observed *in vivo* but not in *in vitro* study, highlighting the importance of the complex liver microenvironment in shaping the metabolic adaptations.

Although increasing saturated FA (palmitate and stearate) levels by modulating NAD^+ metabolism by NAM mononucleotide or NAM riboside supplementation have shown to ameliorate hepatic metabolic disturbances in mice with NAFLD (52), potential therapeutic strategies to retore lipid homeostasis and mitigate the fibrogenic response should targeted the AMPK-SIRT1-SREBP axis. Approaches that aim to activate AMPK have shown promise in preventing lipogenesis and NAFLD (53). However, the role of NF-*κ*B in the liver is complex,

and its inhibition may have both beneficial and detrimental effects, warranting a cautious approach (54).

This comprehensive multi-omics study has revealed the complex dysregulation of NAD^+ metabolism and its profound impact on the metabolic and signaling networks during the progression of liver fibrosis and inflammation-associated HCC. The depletion of NAM levels, despite the upregulation of *de novo* NAD^+ biosynthesis, appears to be a critical driver of the pathological changes. This NAM depletion disrupts the AMPK-SIRT1 axis, leading to the aberrant activation of pro-inflammatory NF-κB signaling in the HSCs. Furthermore, the rewiring of NAD^+ metabolism also contributes to the imbalance in hepatic lipid homeostasis through the AMPK-SIRT1-NF-κB-SREBP axis. This study provides valuable insights into the complex metabolic reprogramming that occurs during the various stages of HCC progression, offering new avenues for the development of targeted therapeutic interventions and early diagnosis.

METHODS

All experiments with mice were approved by the University of Hong Kong (HKU)'s Committee on the Use of Live Animals in Teaching and Research (CULATR), in accordance with the Animals (Control of Experiments) Ordinance of Hong Kong. Procedural details, including disease modeling, metabolomics, lipidomics, transcriptomics, details of QC and bioinformatics for the omics data, are in *SI Appendix*. Python v.3.11 on Jupyter Notebook (Anaconda3), R version 4.3.3 on RStudio 2023.12.1+402, and Microsoft Excel 2024 were used for statistical analyses and data visualization.

Data, Materials, and Software Availability.

All study data are included in the article and/or supporting information. Processed MS and RNA-Seq data (Datasets S1–S5) are available on Zenodo (see 10.5281/zenodo.15593732).

ACKNOWLEDGEMENTS

H. Yan thanks the Start-up Grant for New Academics – YAN Hong (165520). The authors from Hong Kong Baptist University appreciate the contributions made by C.C.-L.'s team in developing and preparing the animal models.

ABBREVIATIONS

3-HAA	3-Hydroxyanthranilate
AAG	Alanine/aspartate/glutamate
Acat2	Acyl-CoA:cholesterol acyltransferase 2
Acly	ATP citrate lyase
AMC	Age-matched control
Aox1	Aldehyde oxidase 1
BA	Bile acid
CCl4	Carbon tetrachloride
Cpt1a	Carnitine palmitoyltransferase 1A
DEG	Differentially expressed gene
DEN	Diethylnitrosamine
DG	Diglyceride
DNL	De novo lipogenesis
ESI	Electrospray ionization
FA	Fatty acid
FAO	Fatty acid oxidation
Fasn	Fatty acid synthase
Haao	3-Hydroxyanthranilate 3,4-dioxygenase
HBV	Hepatitis B virus
HCC	Hepatocellular carcinoma
Hmgcr	3-Hydroxy-3-methylglutaryl-CoA reductase
Hmgcs1	3-Hydroxy-3-methylglutaryl-CoA synthase 1
HSC	Hepatic stellate cell
IFN-γ	Interferon gamma
m/z	Mass-to-charge ratio
MS	Mass spectrometry
NA	Nicotinic acid
NAD^+	Nicotinamide adenine dinucleotide
NAFLD	Non-alcoholic fatty liver disease
NAM	Nicotinamide
Nampt	Nicotinamide phosphoribosyltransferase
NASH	Non-alcoholic steatohepatitis
Nfkb1	Nuclear factor kappa B subunit 1
Nmnat1	Nicotinamide mononucleotide adenylyltransferase 1
Nnmt	Nicotinamide N-methyltransferase

Prkag2	5'-AMP-activated protein kinase subunit gamma-2
QC	Quality control
Qprt	Quinolinate phosphoribosyl transferase
RNA-Seq	RNA sequencing
RPLC	Reverse-phase liquid chromatography
Sirt	Sirtuin
Srebf1	Sterol regulatory element-binding protein 1
Srebf2	Sterol regulatory element-binding protein 2
SREBP	Sterol regulatory element-binding protein
Tdo2	Tryptophan 2,3-dioxygenase
TG	Triglyceride
TGF-β1	Transforming growth factor beta 1

AUTHOR INFORMATION

Disclosure

The authors declare that they have no conflicts of interest or personal relationships that could influence the work reported in this paper.

Author Contributions

Conceptualization, H.-L. N., H. Y., and Z. C.; Resources, H.-L. N., H. Y., C.C.-L. W., and Z. C.; Data Curation, H.-L. N.; Writing-Original Draft Preparation, H.-L. N. and H. Y.; Writing-Review and Editing, H.-L. N., H. Y., J.W.-S. C., K.K.-L. K.; Visualization, H.-L. N., J.W.-S. C., K.K.-L. K.; Supervision, H. Y., C.C.-L. W., and Z. C.; Project Administration, H. Y., C.C.-L. W., and Z. C.; Funding acquisition, H. Y., C.C.-L. W., and Z. C. All authors have read and agreed to the published version of the manuscript.

REFERENCES

1. J. Ferlay, *et al.*, Global Cancer Observatory: Cancer Today. Lyon, France: International Agency for Research on Cancer. *Lyon, France: International Agency for Research on Cancer* 419 (2020). Available at: https://gco.iarc.fr/today [Accessed 6 October 2023].
2. J. M. Llovet, A. Villanueva, A. Lachenmayer, R. S. Finn, Advances in targeted therapies for hepatocellular carcinoma in the genomic era. *Nat Rev Clin Oncol* 12, 408–424 (2015).
3. H. Sung, *et al.*, Global cancer statistics 2020: GLOBOCAN estimates of incidence and mortality worldwide for 36 cancers in 185 countries. *CA Cancer J Clin* 71, 209–249 (2021).
4. A. C. S. The American Cancer Society medical and editorial content team, “Liver cancer early

detection, diagnosis, and staging."
5. L. Laursen, A preventable cancer. *Nature* 516, S3–S4 (2014).
6. G. Fattovich, T. Stroffolini, I. Zagni, F. Donato, Hepatocellular carcinoma in cirrhosis: Incidence and risk factors. *Gastroenterology* 127, S35–S50 (2004).
7. A. G. Singal, H. B. El-Serag, Hepatocellular carcinoma from epidemiology to prevention: Translating knowledge into practice. *Clinical Gastroenterology and Hepatology* 13, 2140 (2015).
8. D. Dhar, J. Baglieri, T. Kisseleva, D. A. Brenner, Mechanisms of liver fibrosis and its role in liver cancer. *Exp Biol Med* 245, 96–108 (2020).
9. D. Y. Zhang, S. L. Friedman, Fibrosis-dependent mechanisms of hepatocarcinogenesis. *Hepatology* 56, 769–775 (2012).
10. P. Luo, *et al.*, A Large-scale, multicenter serum metabolite biomarker identification study for the early detection of hepatocellular carcinoma. *Hepatology* 67, 662–675 (2018).
11. M. Lewinska, *et al.*, The altered serum lipidome and its diagnostic potential for non-alcoholic fatty liver (NAFL)-associated hepatocellular carcinoma: diagnosis of NAFLD-HCC utilising serum lipidomics. *EBioMedicine* 73, 103661 (2021).
12. E. Loftfield, *et al.*, Novel biomarkers of habitual alcohol intake and associations with risk of pancreatic and liver cancers and liver disease mortality. *J Natl Cancer Inst* 113, 1542–1550 (2021).
13. Q. Huang, *et al.*, Metabolic characterization of hepatocellular carcinoma using nontargeted tissue metabolomics. *Cancer Res* 73, 4992–5002 (2013).
14. Y. Lu, *et al.*, Acetylcarnitine is a candidate diagnostic and prognostic biomarker of hepatocellular carcinoma. *Cancer Res* 76, 2912–2920 (2016).
15. T. Feng, *et al.*, Non-invasive assessment of liver fibrosis by serum metabolites in non-human primates and human patients. *iScience* 26, 107538 (2023).
16. D. Beyoğlu, *et al.*, Tissue metabolomics of hepatocellular carcinoma: Tumor energy metabolism and the role of transcriptomic classification. *Hepatology* 58, 229–238 (2013).
17. J. Chaisaingmongkol, *et al.*, Common molecular subtypes among Asian hepatocellular carcinoma and cholangiocarcinoma. *Cancer Cell* 32, 57–70 (2017).
18. M. J. He, *et al.*, Spatial metabolomics on liver cirrhosis to hepatocellular carcinoma progression. *Cancer Cell Int* 22, 366 (2022).
19. X. He, *et al.*, Metabolomic profiling for histologically fibrotic stage in chronic drug-induced liver injury. *Front Pharmacol* 13, 896198 (2022).
20. S. T. Wu, *et al.*, An update on animal models of liver fibrosis. *Front Med (Lausanne)* 10, 1160053 (2023).
21. T. Uehara, I. P. Pogribny, I. Rusyn, The DEN and CCl4-induced mouse model of fibrosis and inflammation-associated hepatocellular carcinoma. *Curr Protoc* 1, e211 (2021).
22. L. W. Sumner, *et al.*, Proposed minimum reporting standards for chemical analysis: Chemical Analysis Working Group (CAWG) Metabolomics Standards Initiative (MSI). *Metabolomics* 3, 211–221 (2007).
23. H. L. Ngan, K. Y. Lam, Z. Li, J. Zhang, Z. Cai, Machine learning facilitates the application of mass spectrometry-based metabolomics to clinical analysis: A review of early diagnosis of high mortality rate cancers. *TrAC - Trends in Analytical Chemistry* 168, 117333 (2023).
24. M. Hoshi, *et al.*, Kynurenine produced by indoleamine 2,3-dioxygenase 2 exacerbates acute liver injury by carbon tetrachloride in mice. *Toxicology* 438, 152458 (2020).
25. M. Komatsu, *et al.*, NNMT activation can contribute to the development of fatty liver disease by modulating the NAD + metabolism. *Sci Rep* 8, 8637 (2018).
26. N. Xie, *et al.*, NAD+ metabolism: Pathophysiologic mechanisms and therapeutic potential. *Signal Transduct Target Ther* 5, 227 (2020).
27. M. F. Fondevila, *et al.*, Inhibition of carnitine palmitoyltransferase 1A in hepatic stellate cells protects against fibrosis. *J Hepatol* 77, 15–28 (2022).
28. S. Satapati, *et al.*, Elevated TCA cycle function in the pathology of diet-induced hepatic insulin resistance and fatty liver. *J Lipid Res* 53, 1080–1092 (2012).
29. H. Chang, *et al.*, Identification of key metabolic changes during liver fibrosis progression in rats using a urine and serum metabolomics approach. *Sci Rep* 7, 11433 (2017).
30. J. Clària, *et al.*, Orchestration of tryptophan-kynurenine pathway, acute decompensation, and acute-on-chronic liver failure in cirrhosis. *Hepatology* 69, 1686–1701 (2019).
31. J. P. Carson, M. W. Robinson, G. A. Ramm, G. N. Gobert, RNA sequencing of LX-2 cells treated with TGF-β1 identifies genes associated with hepatic stellate cell activation. *Mol Biol Rep* 48, 7677–

7688 (2021).
32. T. Tsuchida, S. L. Friedman, Mechanisms of hepatic stellate cell activation. *Nat Rev Gastroenterol Hepatol* 14, 397–411 (2017).
33. Z. Beyzaei, F. Ezgu, B. Geramizadeh, A. Alborzi, A. Shojazadeh, Novel PRKAG2 variant presenting as liver cirrhosis: Report of a family with 2 cases and review of literature. *BMC Med Genomics* 14, 33 (2021).
34. M. Berg, *et al.*, 3-Hydroxyanthralinic acidmetabolismcontrols the hepatic SREBP/lipoprotein axis, inhibits inflammasome activation in macrophages, and decreases atherosclerosis in Ldlr-/- mice. *Cardiovasc Res* 116, 1948–1957 (2020).
35. S. Shen, *et al.*, SIRT1/SREBPs-mediated regulation of lipid metabolism. *Pharmacol Res* 199, 107037 (2024).
36. T. Matsukawa, *et al.*, Hepatic FASN deficiency differentially affects nonalcoholic fatty liver disease and diabetes in mouse obesity models. *JCI Insight* 8, e161282 (2023).
37. W. Wang, C. Yang, T. Wang, H. Deng, Complex roles of nicotinamide N-methyltransferase in cancer progression. *Cell Death Dis* 13, 267 (2022).
38. M. A. Eckert, *et al.*, Proteomics reveals NNMT as a master metabolic regulator of cancer-associated fibroblasts. *Nature* 569, 723–728 (2019).
39. P. Pissios, Nicotinamide N-methyltransferase: More than a vitamin B3 clearance enzyme. *Trends in Endocrinology and Metabolism* 28, 340–353 (2017).
40. R. Cuomo, *et al.*, Nicotinamide methylation in patients with cirrhosis. *J Hepatol* 20, 138–142 (1994).
41. S. J. Mitchell, *et al.*, Nicotinamide improves aspects of healthspan, but not lifespan, in mice. *Cell Metab* 27, 667-676.e4 (2018).
42. A. S. Warden, *et al.*, Elevated brain manganese induces motor disease by upregulating the kynurenine pathway of tryptophan metabolism. *Proc Natl Acad Sci U S A* 122, e2423628122 (2025).
43. Y. Liu, *et al.*, Association of NAD+ levels with metabolic disease in a community-based study. *Front Endocrinol (Lausanne)* 14, 1164788 (2023).
44. W. S. Song, *et al.*, Nicotinic acid riboside maintains NAD+ homeostasis and ameliorates aging-associated NAD+ decline. *Cell Metab* S1550-4131, 00217–7 (2025).
45. A. Balaphas, *et al.*, Optimized isolation and characterization of C57BL/6 mouse hepatic stellate cells. *Cells* 11, 1379 (2022).
46. B. Shi, *et al.*, Heavy-chain antibody targeting of CD38 NAD+ hydrolase ectoenzyme to prevent fibrosis in multiple organs. *Sci Rep* 13, 22085 (2023).
47. Y. Tao, *et al.*, Comprehensive proteomics analysis identifies CD38-mediated NAD+ decline orchestrating renal fibrosis in pediatric patients with obstructive nephropathy. *Molecular and Cellular Proteomics* 22, 100510 (2023).
48. M. Dall, *et al.*, Hepatocyte-specific perturbation of NAD+ biosynthetic pathways in mice induces reversible nonalcoholic steatohepatitis-like phenotypes. *Journal of Biological Chemistry* 297, 101388 (2021).
49. M. Yan, Y. Cui, Q. Xiang, Metabolism of hepatic stellate cells in chronic liver diseases: emerging molecular and therapeutic interventions. *Theranostics* 15, 1715–1740 (2025).
50. N. Koundouros, G. Poulogiannis, Reprogramming of fatty acid metabolism in cancer. *Br J Cancer* 122, 4–22 (2019).
51. Z. Liu, *et al.*, CPT1A-mediated fatty acid oxidation confers cancer cell resistance to immune-mediated cytolytic killing. *Proc Natl Acad Sci U S A* 120, e2302878120 (2023).
52. J. Zhang, F. Chen, Integrated transcriptome and metabolome study reveal the therapeutic effects of nicotinamide riboside and nicotinamide mononucleotide on nonalcoholic fatty liver disease. *Biomedicine and Pharmacotherapy* 175, 116701 (2024).
53. A. Woods, *et al.*, Liver-specific activation of AMPK prevents steatosis on a High-fructose diet. *Cell Rep* 18, 3043–3051 (2017).
54. T. Luedde, R. F. Schwabe, NF-κB in the liver-linking injury, fibrosis and hepatocellular carcinoma. *Nat Rev Gastroenterol Hepatol* 8, 108–118 (2011).

FIGURES

Figure 1: Untargeted metabolomics of the DEN-CCl_4-treated mice liver with liver fibrosis, cirrhosis, and hepatocellular carcinoma. (*A*) Mass spectrometry data acquired in positive and (*B*) negative electrospray ionization mode. Significant metabolites from each disease stage were annotated in level 3 chemical identification confidence with a relative standard deviation (RSD) of < 30% among quality control samples (QCs). Data were represented by the ratio of signal intensity of disease group to of control group, z-score normalized to normal livers.

Figure 2: Pathway enrichment for the DEN-CCl_4-treated mice liver with liver fibrosis, cirrhosis, and hepatocellular carcinoma. The discriminative metabolic pathways enriched from (*A*) metabolomics data and (*B*) RNA sequencing data for hepatic fibrosis, from (*C*) metabolomics data for cirrhotic liver, and (*D*) metabolomics data for carcinogenic liver. The NAD^+-related pathways are highlighted.

Figure 3. Stage-sensitive metabolomic and lipidomic changes along liver fibrosis, cirrhosis, and hepatocellular carcinoma. (*A*) A summary of the multi-omics data for the fibrotic mouse livers. Upregulated genes and metabolites are red-colored. Downregulated genes and metabolites are blue-colored. Non-measured metabolites are grey-colored. Bold text indicated statistical significance with *P*-value < 0.05. Stage-sensitive alterations in metabolites and lipids in (*B*) tryptophan metabolism, (*C*) nicotinate and nicotinamide metabolism, (*D*) fatty acid metabolism, (*E*) alanine, aspartate, glutamate metabolism, and (*F*) citrate cycle. Potential biomarkers are dash-highlighted with red grid lines. *Abbreviations: AMC, Age-matched controls; FIB, Fibrosis; CIR, Cirrhosis; HCC, Hepatocellular carcinoma; ^, P < 0.1; *, P < 0.05; **, P < 0.01; ***, P < 0.001.*

Figure 4. Stage-sensitive metabolomic changes in serum along liver fibrosis, cirrhosis, and hepatocellular carcinoma. (*A*) A summary of the metabolites in tryptophan-kynurenine pathway and NAD^+ metabolism in the fibrotic mice serum. Upregulated metabolites are red-colored. Downregulated metabolites are blue-colored. Non-measured metabolites are grey-colored. Bold text indicated statistical significance with *p*-value < 0.05. Stage-sensitive alterations in metabolites and lipids in (*B*) tryptophan metabolism, and (*C*) nicotinate and nicotinamide metabolism. Potential biomarkers are dash-highlighted with red grid lines. *Abbreviations: AMC, Age-matched controls; FIB, Fibrosis; CIR, Cirrhosis; HCC, Hepatocellular carcinoma; ^, P < 0.1; *, P < 0.05; **, P < 0.01; ***, P < 0.001.*

Figure 5: NAD^+ metabolism and *de novo* NAD^+ biosynthesis pathway in hepatic stellate cells. (*A*) A summary of the genes in *de novo* NAD^+ biosynthesis pathway and NAD^+ metabolism that aligned with the changes with the *in vivo* studies. Upregulated genes are red-colored. Downregulated genes are blue-colored. Bold text indicated statistical significance with *p*-value < 0.05. *In vitro* and *in vivo* differentially expressed genes were represented (*B*) by box plots and (*C–F*) by volcano plots. *Abbreviations: Ctrl, Experimental control; Treat, TGF-β1-activated human HSC cell line LX-2 cells; AMC, Age-matched controls; FIB, Fibrosis; ^, P < 0.1; *, P < 0.05; **, P < 0.01; ***, P < 0.001.*

Figure 6: *De novo* lipogenesis and cholesterogenesis pathway in hepatic stellate cells. (*A*) A summary of the genes in *de novo* lipogenesis and cholesterogenesis pathway that aligned with the changes with the *in vivo* studies. Upregulated genes are red-colored. Downregulated genes are blue-colored. Bold text indicated statistical significance with *p*-value < 0.05. *In vitro* and *in vivo* differentially expressed genes were represented (*B*) by box plots and (*C–F*) by volcano plots. Serum lipids are dash-highlighted with purple

grid lines. *Abbreviations: Ctrl, Experimental control; Treat, TGF-β1-activated human HSC cell line LX-2 cells; AMC, Age-matched controls; FIB, Fibrosis; CIR, Cirrhosis; HCC, Hepatocellular carcinoma; ^, P < 0.1; *, P < 0.05; **, P < 0.01; ***, P < 0.001.*

Figure 1

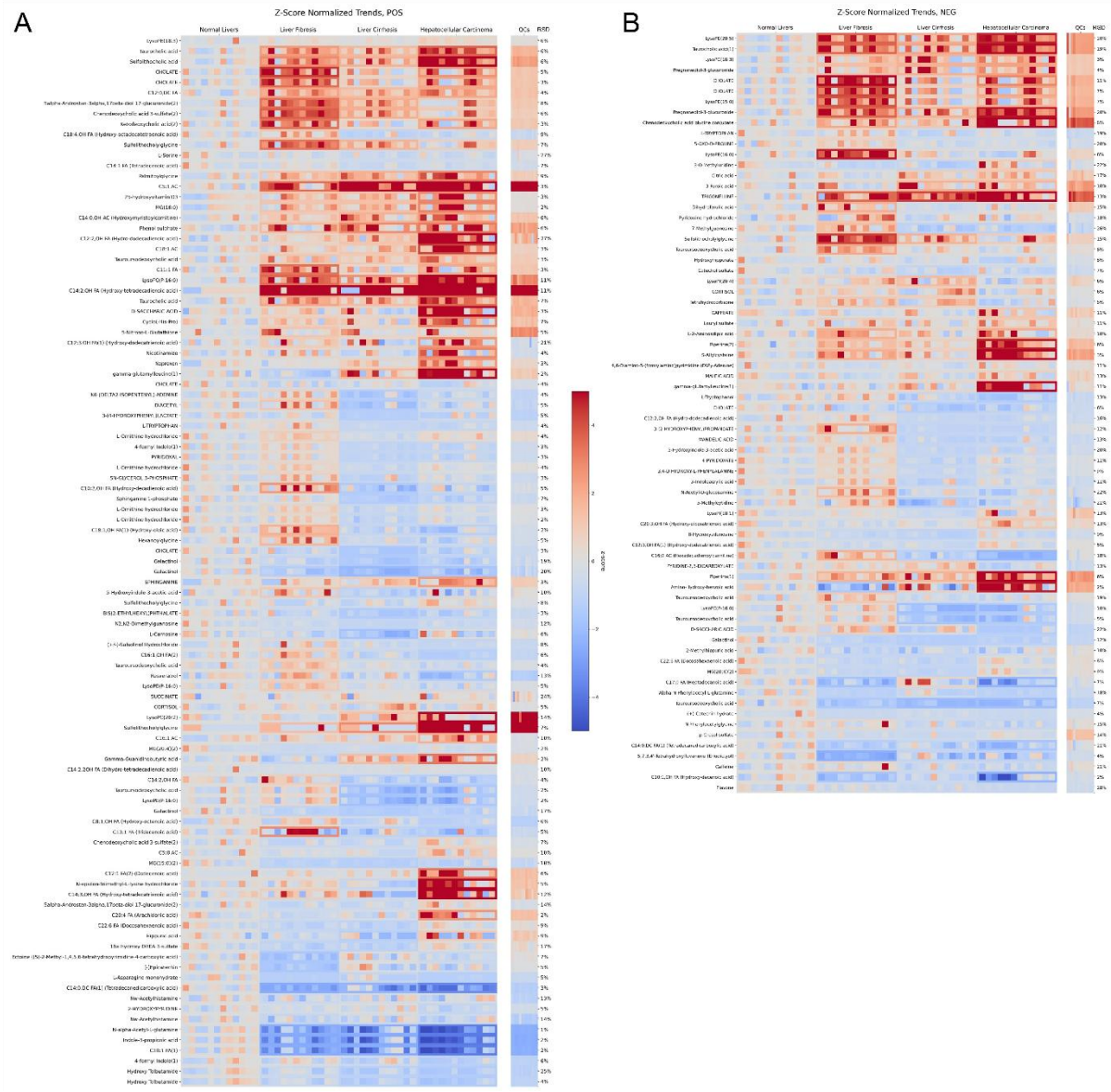
A
Z-Score Normalized Trends, POS
Normal Livers
Liver Fibrosis
Liver Cirrhosis
Hepatocellular Carcinoma
OCs
RSD
B
Z-Score Normalized Trends, NEG
Normal Livers
Liver Fibrosis
Liver Cirrhosis
Hepatocellular Carcinoma
OCs
RSD

Figure 2

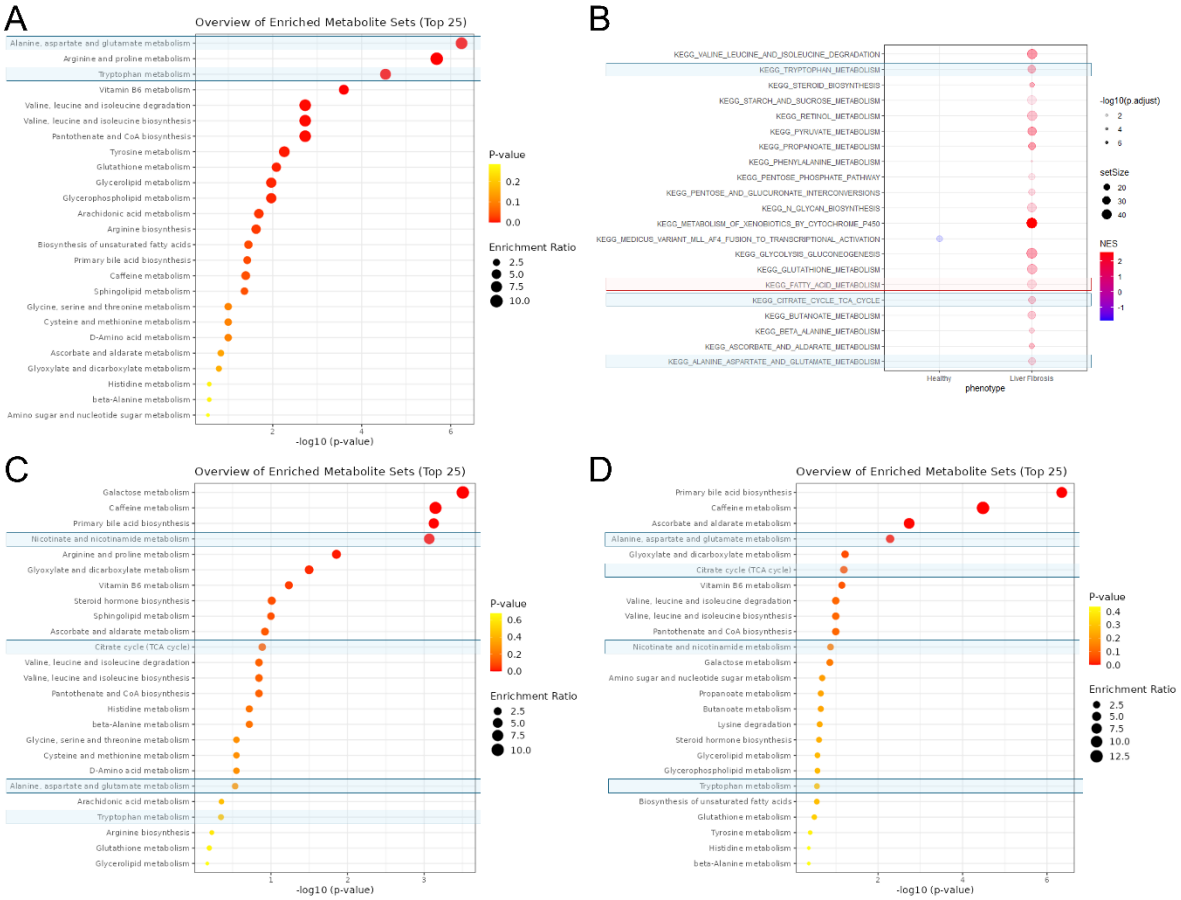
A
Overview of Enriched Metabolite Sets (Top 25)
Alanine, aspartate and glutamate metabolism
Arginine and proline metabolism
Tryptophan metabolism
Vitamin B6 metabolism
Valine, leucine and isoleucine degradation
Valine, leucine and isoleucine biosynthesis
Pantothenate and CoA biosynthesis
Tyrosine metabolism
Glutathione metabolism
Glycerolipid metabolism
Glycerophospholipid metabolism
Arachidonic acid metabolism
Arginine biosynthesis
Biosynthesis of unsaturated fatty acids
Primary bile acid biosynthesis
Caffeine metabolism
Sphingolipid metabolism
Glycine, serine and threonine metabolism
Cysteine and methionine metabolism
D-Amino acid metabolism
Ascorbate and aldarate metabolism
Glyoxylate and dicarboxylate metabolism
Histidine metabolism
beta-Alanine metabolism
Amino sugar and nucleotide sugar metabolism
-log10 (p-value)
P-value
0.2
0.1
0.0
Enrichment Ratio
2.5
5.0
7.5
10.0
B
KEGG_VALINE_LEUCINE_AND_ISOLEUCINE_DEGRADATION
KEGG_TRYPTOPHAN_METABOLISM
KEGG_STEROID_BIOSYNTHESIS
KEGG_STARCH_AND_SUCROSE_METABOLISM
KEGG_RETINOL_METABOLISM
KEGG_PYRUVATE_METABOLISM
KEGG_PROPANOATE_METABOLISM
KEGG_PHENYLALANINE_METABOLISM
KEGG_PENTOSE_PHOSPHATE_PATHWAY
KEGG_PENTOSE_AND_GLUCURONATE_INTERCONVERSIONS
KEGG_N_GLYCAN_BIOSYNTHESIS
KEGG_METABOLISM_OF_XENOBIOTICS_BY_CYTOCHROME_P450
KEGG_MEDICUS_VARIANT_MLL_AF4_FUSION_TO_TRANSCRIPTIONAL_ACTIVATION
KEGG_GLYCOLYSIS_GLUCONEOGENESIS
KEGG_GLUTATHIONE_METABOLISM
KEGG_FATTY_ACID_METABOLISM
KEGG_CITRATE_CYCLE_TCA_CYCLE
KEGG_BUTANOATE_METABOLISM
KEGG_BETA_ALANINE_METABOLISM
KEGG_ASCORBATE_AND_ALDARATE_METABOLISM
KEGG_ALANINE_ASPARTATE_AND_GLUTAMATE_METABOLISM
Healthy
Liver Fibrosis
phenotype
-log10(p.adjust)
setSize
NES
C
Overview of Enriched Metabolite Sets (Top 25)
Galactose metabolism
Caffeine metabolism
Primary bile acid biosynthesis
Nicotinate and nicotinamide metabolism
Arginine and proline metabolism
Glyoxylate and dicarboxylate metabolism
Vitamin B6 metabolism
Steroid hormone biosynthesis
Sphingolipid metabolism
Ascorbate and aldarate metabolism
Citrate cycle (TCA cycle)
Valine, leucine and isoleucine degradation
Valine, leucine and isoleucine biosynthesis
Pantothenate and CoA biosynthesis
Histidine metabolism
beta-Alanine metabolism
Glycine, serine and threonine metabolism
Cysteine and methionine metabolism
D-Amino acid metabolism
Alanine, aspartate and glutamate metabolism
Arachidonic acid metabolism
Tryptophan metabolism
Arginine biosynthesis
Glutathione metabolism
Glycerolipid metabolism
-log10 (p-value)
P-value
0.6
0.4
0.2
0.0
Enrichment Ratio
2.5
5.0
7.5
10.0
D
Overview of Enriched Metabolite Sets (Top 25)
Primary bile acid biosynthesis
Caffeine metabolism
Ascorbate and aldarate metabolism
Alanine, aspartate and glutamate metabolism
Glyoxylate and dicarboxylate metabolism
Citrate cycle (TCA cycle)
Vitamin B6 metabolism
Valine, leucine and isoleucine degradation
Valine, leucine and isoleucine biosynthesis
Pantothenate and CoA biosynthesis
Nicotinate and nicotinamide metabolism
Galactose metabolism
Amino sugar and nucleotide sugar metabolism
Propanoate metabolism
Butanoate metabolism
Lysine degradation
Steroid hormone biosynthesis
Glycerolipid metabolism
Glycerophospholipid metabolism
Tryptophan metabolism
Biosynthesis of unsaturated fatty acids
Glutathione metabolism
Tyrosine metabolism
Histidine metabolism
beta-Alanine metabolism
-log10 (p-value)
P-value
0.4
0.3
0.2
0.1
0.0
Enrichment Ratio
2.5
5.0
7.5
10.0
12.5

Figure 3

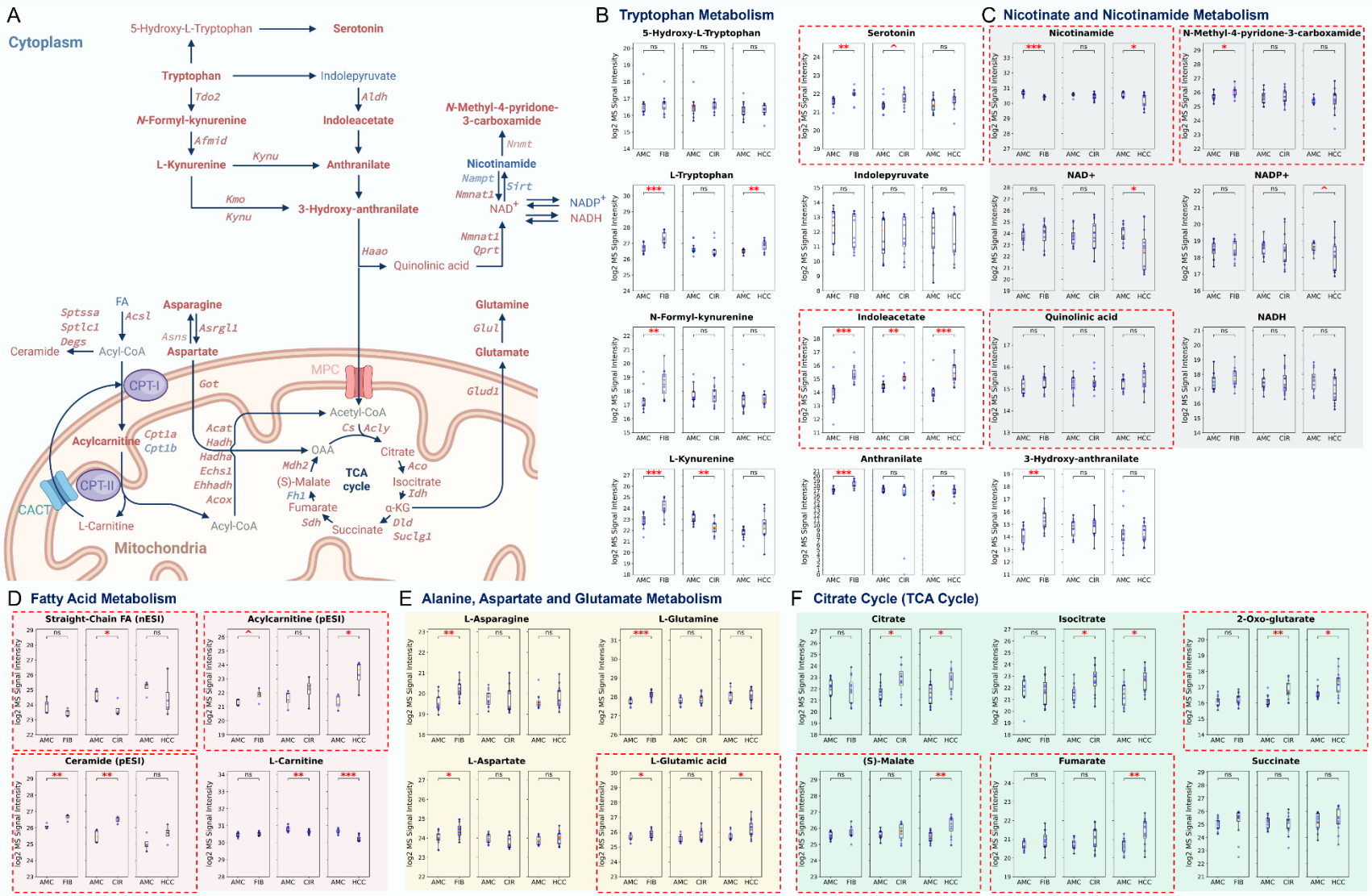
A
Cytoplasm
5-Hydroxy-L-Tryptophan
Serotonin
Tryptophan
Indolepyruvate
Tdo2
Aldh
N-Formyl-kynurenine
Indoleacetate
N-Methyl-4-pyridone-3-carboxamide
Afmid
Nnmt
L-Kynurenine
Kynu
Anthranilate
Nicotinamide
Nampt
Sirt
Nmnat1
Kmo
Kynu
3-Hydroxy-anthranilate
NAD+
NADP+
NADH
Nmnat1
Qprt
Haao
Quinolinic acid
FA
Acsl
Asparagine
Sptssa
Sptlc1
Degs
Asns
Asrgl1
Glutamine
Glul
Ceramide
Acyl-CoA
Aspartate
Glutamate
MPC
Got
Glud1
CPT-I
Acetyl-CoA
Acat
Hadh
Hadha
Echs1
Ehhadh
Acox
Cs
Acly
Acylcarnitine
Cpt1a
Cpt1b
OAA
Citrate
Mdh2
TCA cycle
Aco
(S)-Malate
Isocitrate
Idh
CPT-II
Fh1
Fumarate
α-KG
CACT
L-Carnitine
Acyl-CoA
Sdh
Succinate
Dld
Suclg1
Mitochondria
B Tryptophan Metabolism
5-Hydroxy-L-Tryptophan
Serotonin
L-Tryptophan
Indolepyruvate
N-Formyl-kynurenine
Indoleacetate
L-Kynurenine
Anthranilate
3-Hydroxy-anthranilate
C Nicotinate and Nicotinamide Metabolism
Nicotinamide
N-Methyl-4-pyridone-3-carboxamide
NAD+
NADP+
Quinolinic acid
NADH
D Fatty Acid Metabolism
Straight-Chain FA (nESI)
Acylcarnitine (pESI)
Ceramide (pESI)
L-Carnitine
E Alanine, Aspartate and Glutamate Metabolism
L-Asparagine
L-Glutamine
L-Aspartate
L-Glutamic acid
F Citrate Cycle (TCA Cycle)
Citrate
Isocitrate
2-Oxo-glutarate
(S)-Malate
Fumarate
Succinate
log2 MS Signal Intensity
AMC
FIB
CIR
HCC

Figure 4

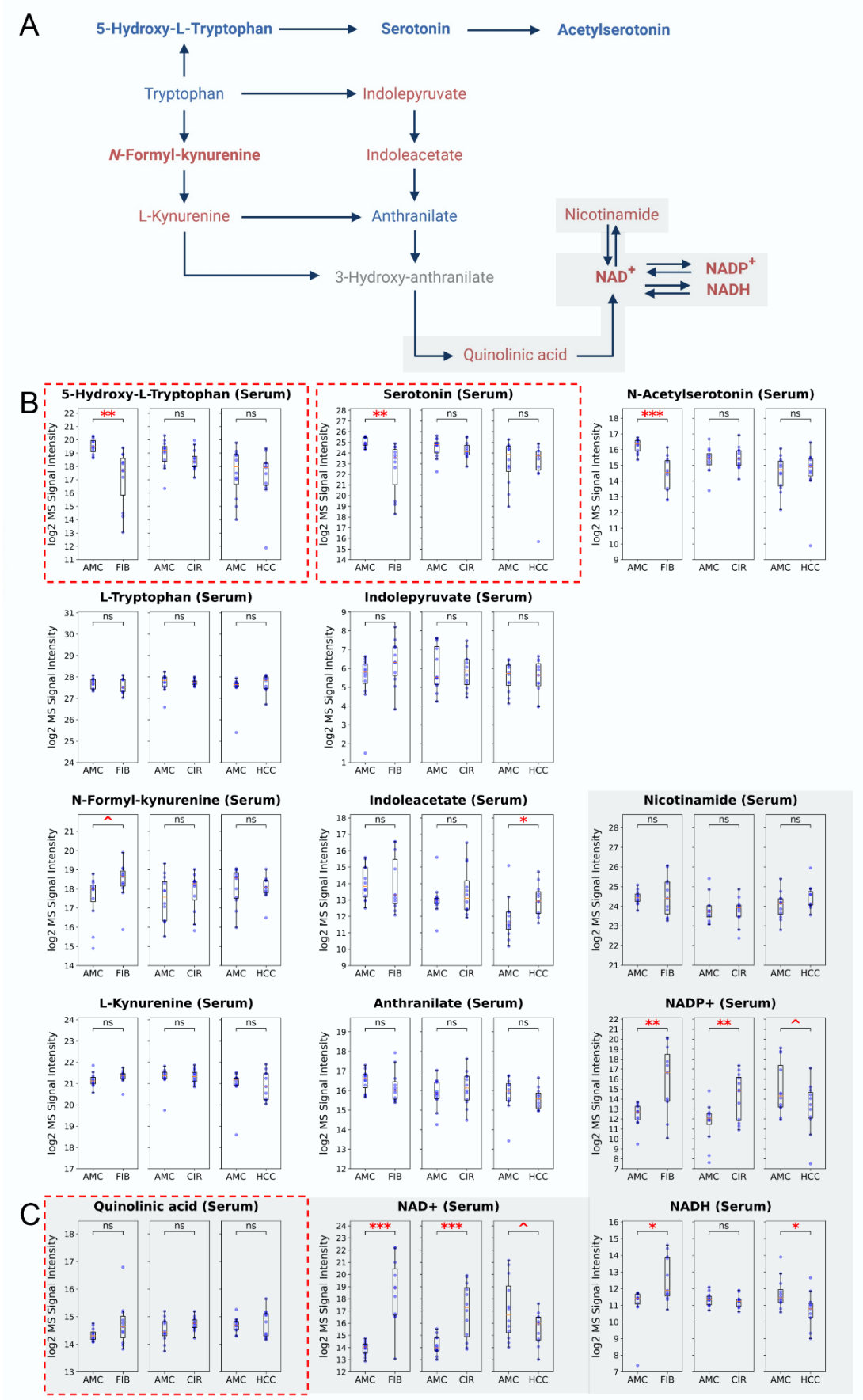
A
5-Hydroxy-L-Tryptophan
Serotonin
Acetylserotonin
Tryptophan
Indolepyruvate
N-Formyl-kynurenine
Indoleacetate
L-Kynurenine
Anthranilate
Nicotinamide
3-Hydroxy-anthranilate
NAD+
NADP+
NADH
Quinolinic acid
B
5-Hydroxy-L-Tryptophan (Serum)
Serotonin (Serum)
N-Acetylserotonin (Serum)
L-Tryptophan (Serum)
Indolepyruvate (Serum)
N-Formyl-kynurenine (Serum)
Indoleacetate (Serum)
Nicotinamide (Serum)
L-Kynurenine (Serum)
Anthranilate (Serum)
NADP+ (Serum)
C
Quinolinic acid (Serum)
NAD+ (Serum)
NADH (Serum)
log2 MS Signal Intensity
AMC
FIB
CIR
HCC
ns

Figure 5

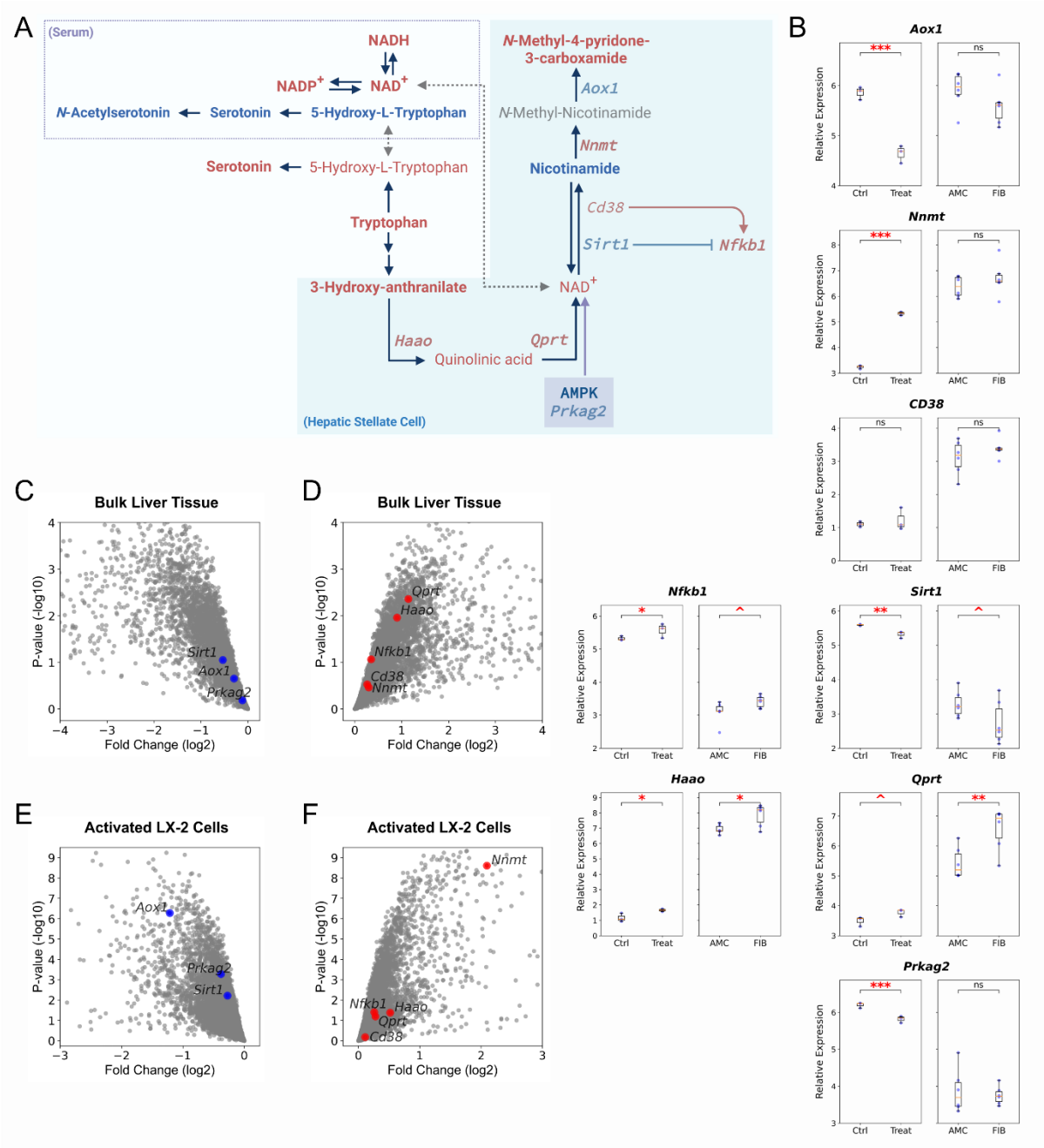
A
(Serum)
NADH
NADP+
NAD+
N-Acetylserotonin
Serotonin
5-Hydroxy-L-Tryptophan
Serotonin
5-Hydroxy-L-Tryptophan
Tryptophan
3-Hydroxy-anthranilate
Haao
Quinolinic acid
Qprt
N-Methyl-4-pyridone-3-carboxamide
Aox1
N-Methyl-Nicotinamide
Nnmt
Nicotinamide
Cd38
Sirt1
Nfkb1
NAD+
AMPK
Prkag2
(Hepatic Stellate Cell)
B
Aox1
Nnmt
CD38
Nfkb1
Sirt1
Haao
Qprt
Prkag2
Relative Expression
Ctrl
Treat
AMC
FIB
C
Bulk Liver Tissue
P-value (-log10)
Fold Change (log2)
Sirt1
Aox1
Prkag2
D
Bulk Liver Tissue
Qprt
Haao
Nfkb1
Cd38
Nnmt
E
Activated LX-2 Cells
Aox1
Prkag2
Sirt1
F
Activated LX-2 Cells
Nnmt
Nfkb1
Haao
Qprt
Cd38

Figure 6

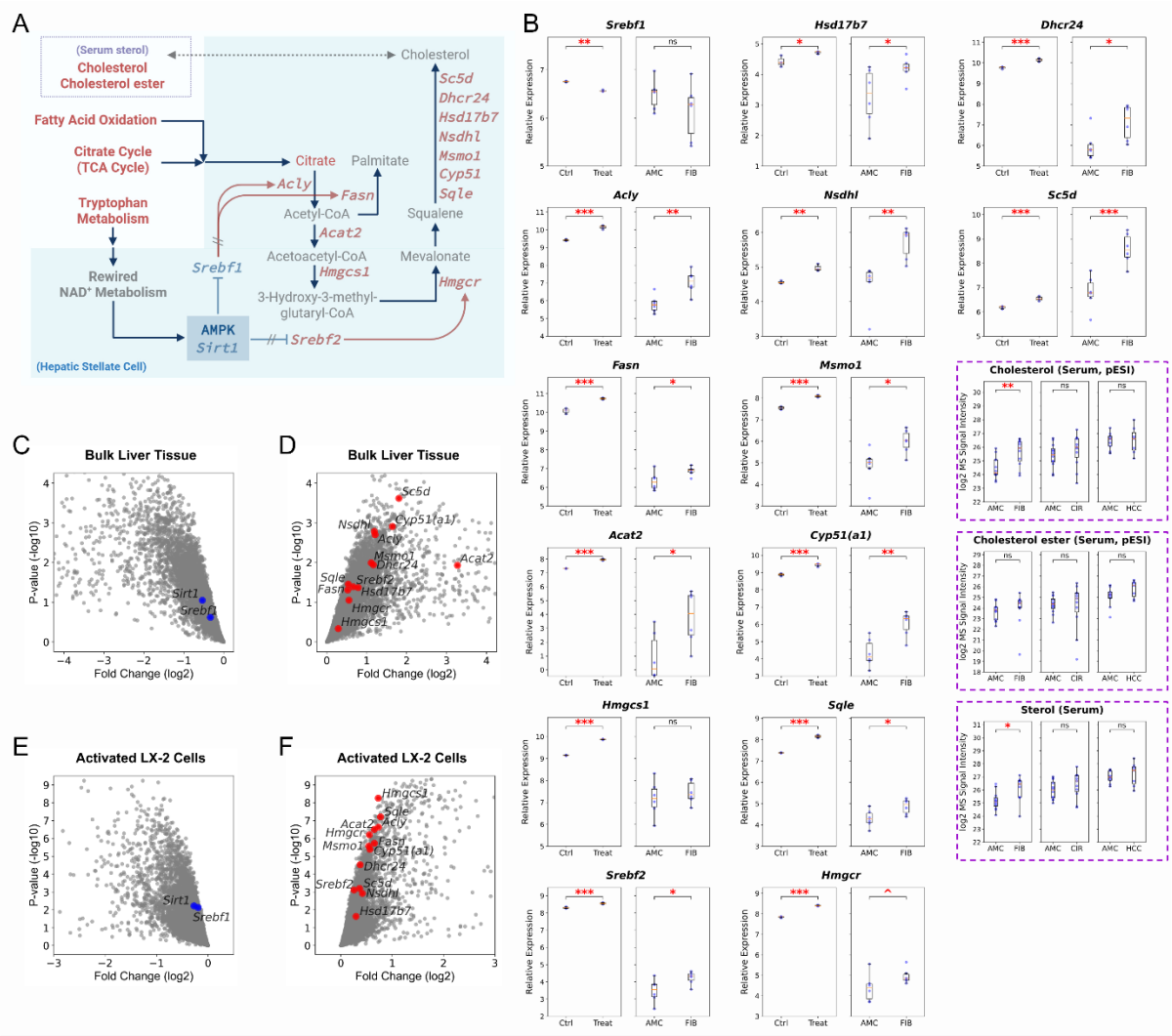
A
(Serum sterol)
Cholesterol
Cholesterol ester
Cholesterol
Sc5d
Dhcr24
Hsd17b7
Nsdhl
Msmo1
Cyp51
Sqle
Fatty Acid Oxidation
Citrate Cycle (TCA Cycle)
Citrate
Palmitate
Acly
Fasn
Tryptophan Metabolism
Acetyl-CoA
Squalene
Acat2
Acetoacetyl-CoA
Mevalonate
Srebf1
Hmgcs1
Hmgcr
Rewired NAD+ Metabolism
3-Hydroxy-3-methyl-glutaryl-CoA
AMPK
Sirt1
Srebf2
(Hepatic Stellate Cell)
B
Srebf1
Hsd17b7
Dhcr24
Acly
Nsdhl
Sc5d
Fasn
Msmo1
Acat2
Cyp51(a1)
Hmgcs1
Sqle
Srebf2
Hmgcr
Cholesterol (Serum, pESI)
Cholesterol ester (Serum, pESI)
Sterol (Serum)
Relative Expression
log2 MS Signal Intensity
Ctrl
Treat
AMC
FIB
CIR
HCC
C
Bulk Liver Tissue
P-value (-log10)
Fold Change (log2)
Sirt1
Srebf1
D
Bulk Liver Tissue
Sc5d
Nsdhl
Cyp51(a1)
Acly
Msmo1
Dhcr24
Acat2
Sqle
Srebf2
Fasn
Hsd17b7
Hmgcr
Hmgcs1
E
Activated LX-2 Cells
F
Activated LX-2 Cells

TABLES

Table 1: Summary of the differentially expressed genes in DEN-CCl_4 mice and TGF-β1-activated human HSC cell line LX-2 cells.

		DEN-CCl_4 Mice			LX-2 Cells		
Pathway	Gene	Fold Change (log2)	*P*-value	Adjusted *P*	Fold Change (log2)	*P*-value	Adjusted *P*
Tryptophan Metabolism	*Tph2*	/	/	/	-0.24	0.151	0.325
	Ddc	-0.03	0.936	0.959	/	/	/
	Il4i1	/	/	/	-0.65	0.070	0.192
	Aldh1b1	1.29	0.001	0.029	0.25	0.079	0.208
	Aldh2	1.72	0.006	0.053	-0.41	0.000	0.003
	Aldh7a1	1.05	0.015	0.079	-0.19	0.009	0.043
	Aldh9a1	0.89	0.022	0.093	0.37	0.000	0.002
	Aldh3a2	1.95	0.034	0.116	-0.04	0.760	0.868
	Tdo2	1.72	0.000	0.029	/	/	/
	Ido1	/	/	/	-0.36	0.368	0.574
	Ido2	0.52	0.140	0.268	0.10	0.633	0.787
	Afmid	0.73	0.033	0.115	0.06	0.546	0.726
	Kmo	1.01	0.011	0.069	-0.01	0.947	0.973
	Kynu	0.67	0.059	0.158	-0.02	0.845	0.918
	Haao	0.90	0.011	0.069	0.52	0.042	0.133
Nicotinate and Nicotinamide Metabolism	*Qprt*	1.14	0.004	0.049	0.28	0.064	0.179
	Nmnat1	0.49	0.063	0.163	-0.07	0.579	0.749
	Nadsyn1	-0.32	0.294	0.442	-0.07	0.371	0.577
	Nampt	-0.38	0.054	0.148	0.58	0.000	0.001
	Nmnat2	/	/	/	-0.40	0.051	0.152
	Nmnat3	-0.05	0.908	0.940	/	/	/
	Nadk	-0.07	0.734	0.819	0.10	0.208	0.401
	Nadk2	-0.01	0.981	0.988	0.19	0.026	0.095
	Nnt	0.75	0.452	0.596	-0.30	0.004	0.023
	Sirt1	-0.54	0.090	0.202	-0.27	0.006	0.033
	Sirt2	-0.46	0.023	0.096	-0.02	0.770	0.874
	Sirt3	0.01	0.957	0.973	-0.28	0.041	0.132
	Sirt4	-0.69	0.015	0.080	/	/	/
	Sirt6	-0.53	0.169	0.306	-0.02	0.835	0.914
	Sirt7	-0.60	0.010	0.065	-0.10	0.220	0.416
	Sarm1	/	/	/	0.28	0.003	0.017
	Bst1	/	/	/	-0.23	0.042	0.134
	Cd38	0.27	0.296	0.444	0.11	0.664	0.808
	Nnmt	0.30	0.345	0.494	2.10	0.000	0.000
	Aox1	-0.30	0.223	0.366	-1.21	0.000	0.000
	Aox3	0.29	0.390	0.537	/	/	/

Citrate Cycle (TCA Cycle)	*Cs*	0.92	0.012	0.071	0.14	0.016	0.067
	Aco1	0.60	0.037	0.121	-0.20	0.017	0.071
	Aco2	0.89	0.037	0.120	0.04	0.859	0.927
	Idh1	1.24	0.006	0.053	-0.07	0.344	0.552
	Idh2	1.12	0.008	0.061	0.01	0.953	0.976
	Idh3g	0.56	0.039	0.124	0.03	0.700	0.831
	Ogdh	0.29	0.209	0.352	0.03	0.681	0.820
	Dlst	2.95	0.117	0.240	0.01	0.842	0.917
	Dld	0.96	0.001	0.033	0.08	0.205	0.397
	Suclg2	2.27	0.128	0.254	-0.56	0.000	0.001
	Suclg1	1.59	0.005	0.051	0.10	0.266	0.469
	Sucla2	0.59	0.184	0.322	0.23	0.458	0.654
	Sdhc	0.74	0.037	0.121	0.01	0.899	0.948
	Sdhd	1.11	0.003	0.044	0.02	0.820	0.905
	Sdha	1.28	0.002	0.038	-0.08	0.120	0.278
	Sdhb	0.73	0.040	0.126	0.00	0.993	0.998
	Fh1	-0.51	0.071	0.175	0.05	0.640	0.792
	Mdh2	1.29	0.004	0.045	0.04	0.520	0.704
Fatty Acid Metabolism	*Pnpla2*	0.56	0.026	0.102	-0.36	0.002	0.013
	Lipe	-1.27	0.008	0.062	-0.44	0.011	0.052
	Mgll	-0.73	0.029	0.107	-0.06	0.608	0.770
Fatty Acid Metabolism / Fatty Acid Degradation	*Acsl5*	2.30	0.000	0.025	-0.34	0.313	0.519
	Acsl3	0.75	0.002	0.040	0.77	0.000	0.000
	Acsl1	-0.30	0.314	0.462	-0.04	0.744	0.857
	Acsl4	0.13	0.548	0.673	0.43	0.001	0.008
	Sptssa	0.70	0.031	0.111	0.04	0.633	0.787
	Sptlc1	0.98	0.002	0.040	0.13	0.210	0.403
	Cers6	-1.69	0.001	0.029	-0.05	0.486	0.676
	Cers4	-1.12	0.025	0.101	-0.03	0.877	0.937
	Degs1	0.84	0.009	0.064	0.01	0.849	0.921
	Cpt1a	0.89	0.011	0.068	-0.51	0.001	0.007
	Cpt1b	-2.12	0.062	0.161	-0.09	0.432	0.632
	Slc25a20	0.04	0.827	0.886	-0.27	0.126	0.287
	Slc25a29	0.23	0.521	0.651	-0.21	0.051	0.153
	Cpt2	0.06	0.852	0.903	-0.10	0.318	0.524
	Acox1	1.04	0.005	0.050	-0.02	0.796	0.891
	Acox3	0.15	0.557	0.680	0.72	0.000	0.002
	Ehhadh	1.60	0.004	0.045	-0.44	0.044	0.139
	Echs1	1.33	0.002	0.037	0.03	0.725	0.847
	Hadha	0.79	0.015	0.080	0.09	0.337	0.544
	Hadh	0.80	0.020	0.090	-0.33	0.037	0.122
	Acaa1	0.18	0.337	0.485	-0.01	0.896	0.947
	Acaa2	1.44	0.003	0.044	-0.35	0.008	0.039
	Hadhb	1.11	0.005	0.051	-0.05	0.561	0.737
	Acat1	0.77	0.033	0.113	-0.09	0.323	0.530

Fatty Acid Metabolism / Mevalonate Pathway	*Acat2*	3.27	0.012	0.071	0.65	0.000	0.000
	Acat3	0.72	0.018	0.085	/	/	/
	Srebf1	-0.33	0.241	0.386	-0.19	0.008	0.039
	Srebf2	0.66	0.041	0.128	0.26	0.001	0.007
	Acly	1.21	0.002	0.037	0.73	0.000	0.000
	Acss2	1.69	0.001	0.029	0.18	0.021	0.082
	Acss3	-0.13	0.557	0.681	-0.86	0.001	0.007
	Fasn	0.52	0.049	0.142	0.65	0.000	0.000
	Hmgcs1	0.29	0.462	0.604	0.73	0.000	0.000
	Hmgcr	0.56	0.089	0.201	0.55	0.000	0.000
Fatty Acid Metabolism / Steroid Biosynthesis	*Mvk*	0.00	0.999	0.999	0.21	0.063	0.176
	Pmvk	1.40	0.062	0.162	-0.26	0.078	0.205
	Mvd	0.04	0.924	0.950	0.87	0.000	0.000
	Sqle	0.54	0.035	0.118	0.77	0.000	0.000
	Fdft1	0.87	0.015	0.079	0.21	0.299	0.504
	Lss	0.78	0.017	0.083	-0.31	0.002	0.014
	Cyp51(a1)	1.64	0.001	0.032	0.56	0.000	0.000
	Tm7sf2	1.74	0.003	0.040	0.00	0.994	0.998
	Lbr	0.56	0.023	0.095	-0.35	0.001	0.006
	Msmo1	1.11	0.010	0.067	0.54	0.000	0.000
	Nsdhl	1.19	0.002	0.035	0.42	0.001	0.010
	Hsd17b7	0.79	0.043	0.131	0.29	0.023	0.088
	Dhcr24	1.17	0.011	0.070	0.38	0.000	0.000
	Sc5d	1.80	0.000	0.024	0.36	0.001	0.006
	Dhcr7	1.12	0.003	0.043	0.67	0.000	0.000
Alanine, Aspartate, and Glutamate Metabolism	*Asns*	0.23	0.674	0.775	0.48	0.000	0.002
	Asrgl1	0.60	0.037	0.121	-0.22	0.195	0.385
	Got1	0.97	0.050	0.143	-0.28	0.012	0.055
	Got2	1.34	0.006	0.056	0.06	0.388	0.593
	Glud1	0.82	0.010	0.066	-0.30	0.008	0.040
	Glul	0.76	0.060	0.159	-0.27	0.006	0.033
AMPK Signaling Pathway / Longevity Regulating Pathway	*Stk11*	-0.65	0.007	0.058	-0.21	0.139	0.306
	Prkaa2	0.31	0.147	0.278	-0.76	0.001	0.009
	Prkab1	-0.07	0.743	0.825	0.00	0.998	0.999
	Prkab2	-0.22	0.589	0.708	0.61	0.000	0.001
	Prkag1	0.25	0.266	0.413	-0.09	0.302	0.507
	Prkag2	-0.12	0.654	0.759	-0.38	0.001	0.001
	Bax	-0.32	0.195	0.336	-0.16	0.041	0.132
	Nfkb1	0.35	0.087	0.198	0.26	0.039	0.127
	Rela	0.18	0.346	0.495	0.15	0.028	0.101
	Ppargc1a	0.74	0.030	0.110	-1.68	0.003	0.018